# Pore-scale imaging and determination of relative permeability and capillary pressure in a mixed-wet carbonate reservoir rock at subsurface conditions

*Amer M.* Alhammadi[*], *Ying* Gao, *Takashi* Akai, *Martin J.* Blunt, and *Branko* Bijeljic

Department of Earth Science and Engineering, Imperial College London, SW7 2AZ, United Kingdom

**Abstract.** We use X-ray micro-tomography combined with a high-pressure high-temperature steady-state flow apparatus to simultaneously measure relative permeability and capillary pressure in a carbonate core from a producing oil field from the Middle East. The native reservoir wettability conditions were restored by ageing the sample at 10 MPa and 80 °C. Imaging and measurement of steady-state relative permeability were performed at eight water fractional flows ($f_w$ = 0, 0.15, 0.3, 0.5, 0.7, 0.85, 0.95, 1), while measuring the pressure differential across the sample. The formation brine was doped with 30 weight % KI to resolve the fluid saturation in the macro- and the sub-resolution pores. The measured relative permeabilities indicated favourable oil recovery with a cross-over saturation above 60%. Below this saturation the water relative permeability is low, while above it oil still flows through thin layers resulting in additional recovery. We quantify oil recovery from both macro-pores and micro-pores. The measurements of the interfacial curvature indicated negative capillary pressure that decreased with an increase in fractional flow, which is a signature of predominantly oil-wet media. Overall, this work has important implications for improved oil recovery in mixed-wet reservoirs. The measured relative permeability, capillary pressure and fluid distribution can also be used to benchmark and validate pore-scale models.

## 1 Introduction

Designing subsurface processes such as hydrocarbon recovery and geological carbon dioxide storage requires an understanding of multiphase fluid flow in natural porous media [1-3] which is described by relative permeability and capillary pressure [1,4-6].

Conventionally, three main special core analysis (SCAL) methods are used to measure capillary pressure. These methods include the centrifuge, the porous plate method, and mercury intrusion capillary pressure, MICP method [5, 7-9]. All of the three methods have advantages and limitations. The centrifuge method, for instance, is difficult to conduct at subsurface conditions and boundary conditions influence the measured data [8]. On the other hand, the porous plate method can produce a homogeneous saturation profile using reservoir fluids. It is also considered reliable for both drainage and waterflood [6, 10]. However, the porous plate method takes a relatively long time to reach capillary equilibrium at every point in the measurement [11]. MICP is cost-effective and can be conducted in a relatively short period of time. However, the sample can be used only once as this method is destructive. In addition, mercury has a different wettability than reservoir rocks and is used to perform drainage only. Finally, this method is limited to small rock samples.

Relative permeability is accurately measured by the steady-state method which applies a sequence of fractional flows ($f_w$) at which the pressure differential due to flow is recorded and the saturation measured from either mass balance or imaging [4, 12]. The relative permeability is usually measured on a different rock sample from the capillary pressure with experiments that employ different displacement methods. Capillary pressure and relative permeability could be measured on the same sample using the semi-dynamic method, however, it is time consuming.

Recently, non-destructive three-dimensional imaging using X-ray micro-tomography has been improved and combined with high-pressure and high-temperature injection to study multiphase flow in permeable media [13-23]. This has facilitated the measurement of relative permeability by accurately measuring the pressure differential across a small rock sample during a steady-state displacement combined with pore-scale imaging. This method has been used to measure relative permeability of a water-wet Bentheimer sandstone [24].

The same pore-scale images used to quantify brine saturation can be used to measure interfacial curvature by capturing the fluid-fluid interface [20, 25] which can then be used to calculate capillary pressure using the Young-Laplace equation. Recently, both capillary pressure and relative permeability have been measured simultaneously

---
[*] Corresponding author: a.alhammadi15@imperial.ac.uk

on the same water-wet Bentheimer sample during a steady-state experiment [26].

However, hydrocarbon reservoirs are rarely water-wet, but instead have mixed-wettability as a result of contacting crude oil [27-29], where parts of the pore space remain water-wet while others through direct contact with the polar components become more oil-wet or neutrally-wet [29, 30]. Relative permeability and capillary pressure are affected by the wettability state of the rock [31-35]. Recently, both water-wet and mixed-wet relative permeability were measured using X-ray images on Bentheimer sandstone saturated with Soltrol-130 as an oil phase [36] which showed an evidence of increased ganglion dynamics at low water saturation. Another complexity arises when studying carbonates, for which characterisation of micro-porosity is necessary since it can enhance pore space connectivity. For this purpose, a differential imaging method was developed for studying single-phase flow [37, 38] and multiphase flow [24, 39]. Gao et al. [40] studied steady-state relative permeability in a water-wet micro-porous limestone. Using differential imaging to characterise fluid occupancy in micro- and macro pore space, it was demonstrated that relative permeability and oil recovery were impacted by water-wet micro-porosity which provided additional connectivity to the water phase.

Nevertheless, all of the studies that used pore-scale imaging to measure relative permeability were conducted on quarry samples and used refined oil at room temperature. To have a thorough understanding of the multiphase flow properties in a mixed-wet reservoir, it is vital to carry out experiments on heterogeneous reservoir rock systems at subsurface conditions.

In this study, we use a complex carbonate reservoir rock extracted from a very large producing oilfield which has a heterogeneous pore structure that is saturated with crude oil and the prepared formation brine from the same reservoir at subsurface conditions. We use the X-ray micro-tomography to acquire pore-scale images from which brine saturation was calculated while measuring pressure drop across the sample to obtain the relative permeability. The same pore-scale images are used to determine the local capillary pressure and fluid occupancy in the pore space.

# 2 Materials and methods

## 2.1 Materials

### 2.1.1 Porous media

Two carbonate reservoir rock samples were drilled and assembled together to make a longer sample (50.1 mm in length) and 6.2 mm in diameter. The rock was mostly calcite $99.8 \pm 0.5$ weight% with small amounts of quartz $0.2 \pm 0.1$ weight%. The chemical composition was measured by X-ray diffraction analysis performed at the Natural History Museum, London, UK. The rock had a total porosity of 27.4% (measured on the X-ray segmented image) and a brine permeability of 292 mD.

### 2.1.2 Oil phase

Crude oil from the same reservoir was used as an oil phase to saturate the sample. The crude oil had a density and viscosity of 812 $kg/m^3$ and 1.94 mP·s respectively, measured at 60 °C. The crude oil contained 55.23% saturates, 38.07% aromatic, 6.22% resins and 0.46% asphaltenes, measured by Weatherford Laboratories.

### 2.1.3 Water (brine) phase

Prepared formation brine was used as the aqueous (water) phase, containing Sodium, Calcium, Magnesium, Chloride, Sulphate and Bicarbonate. After preparing the formation brine, it was doped with 30 weight% Potassium Iodide to resolve water and oil in the sub-resolution pore space. The density and viscosity of the used brine were 1,344 $kg/m^3$ and 0.83 mP·s, respectively measured at 60 °C.

## 2.2 Methodology

### 2.2.1 Core holder assembly and high-pressure high-temperature flow apparatus

Before commencing the flow experiment the carbon fibre core holder assembly had been prepared with dry and clean rock sample, which is described as follows and shown in Figure 1.

• Firstly, two reservoir rock samples were drilled while running tap water as a coolant fluid.

• Both ends of the samples were made flat to have a perfect fit with each other and with the metal end-pieces.

• The samples were solvent-cleaned with a mixture of 50/50 volume% methanol and toluene [41] and dried overnight.

• The dry samples were inserted inside a Viton sleeve.

• The Viton sleeve was connected to the co-injection metal end-piece from the base side and to the top metal end-piece from the top side, which had a tight fit over both end-pieces to avoid confining fluid leaking into the sample.

• The thermocouple was inserted through the base of the core holder and placed carefully next to the sample to measure the pore space temperature.

• A flexible heating jacket was wrapped around the carbon fibre sleeve to elevate the sample temperature.

• Both end-pieces were connected to polyether ether ketone (PEEK) tubing through which crude oil, formation brine and confining DI water were injected. The PEEK tubing was used to allow smooth and flexible rotation of the whole core holder assembly while acquiring X-ray images without shifting the sample.

• Three-way valves were connected to all oil, brine and receiving lines which is considered as a crucial component for the success of the experiment. The combination of three-way valves was used to divert air out of the lines and avoid having any air in the sample.

• Furthermore, the three-way valves were used to isolate the whole core holder assembly in preparation for its transfer into an oven for the ageing process at high pressure and temperature followed by the transfer of the core holder assembly back to the micro-CT enclosure to perform the steady state experiment on the aged sample.

• The completed core holder assembly containing a dry sample is shown in Figure 1.

The next step was performing the steady-state flow experiment using the experimental apparatus shown in Figure 2. A combination of four high pressure syringe pumps was used to apply constant oil and brine flow rates and maintain high pore and confining pressure. The core holder can withstand high pressure and temperature, yet is almost transparent to X-rays [42]. A co-injection end-piece was used to inject both crude oil and formation brine simultaneously into the reservoir rock sample. A proportional-integral-derivative controller (PID) was used to apply constant elevated temperature through a flexible heating jacket. The pressure differential across the rock sample was measured by a 300 kPa pressure transducer.

• Firstly, a confining pressure of 2 MPa was applied to squeeze the Viton sleeve onto the sample to prevent fluids flow on the side of the rock sample. At this stage a dry reference scan was taken.

• The air was removed out of the pore space by injecting carbon dioxide which was followed by brine injection to fully saturate the pores. At this stage a brine reference scan was acquired.

• The absolute permeability was measured by applying five flow rates in single phase brine injection.

• After that the core holder assembly was isolated using the three-way valves and moved to an oven at which primary drainage and ageing was performed at 10 MPa and 80 °C over a period of two weeks to establish the mixed-wettability conditions known to exist in hydrocarbon reservoirs [27-29].

• After completing ageing, the core holder assembly was isolated and moved back carefully into the X-ray micro-tomography scanner.

• The PID controller was connected to the core holder assembly to maintain pore space temperature of $60 \pm 1$ °C. The back pressure valve was set to maintain a pore pressure of 1 MPa while the confining pump applied a confining pressure of 3 MPa.
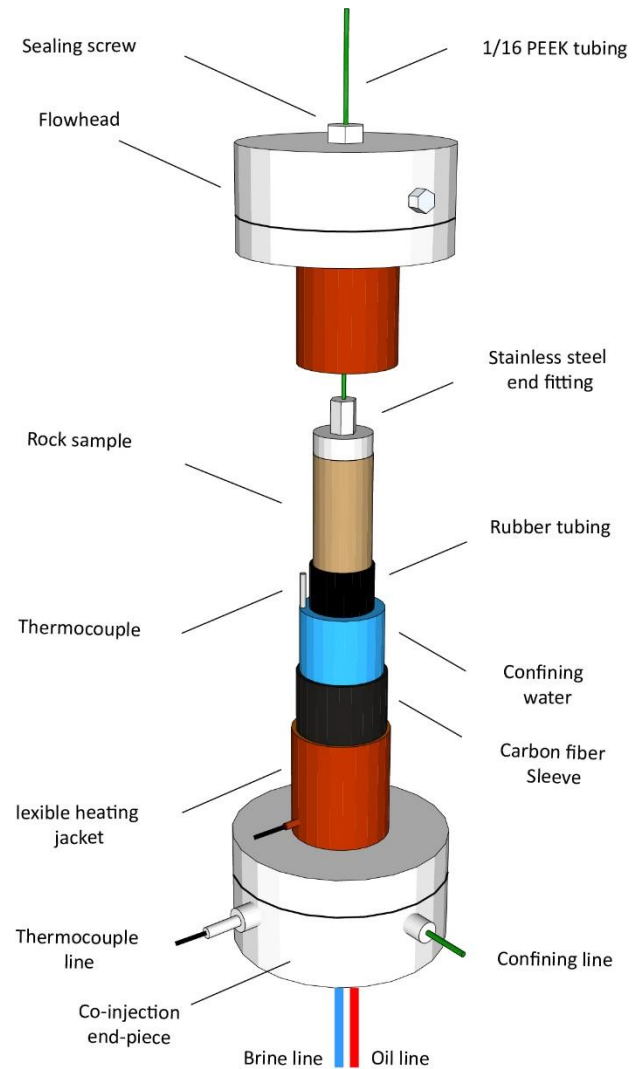


**Fig. 1.** A schematic demonstration of the core holder assembly with the rock sample. All of the core holder assembly components are labelled with the internal cross-section view of the core holder.

• A total of eight brine (water) fractional flows were imposed to measure the relative permeability ($f_w$= 0, 0.15, 0.3, 0.5, 0.7, 0.85, 0.95 and 1). The total co-injection flow rate was 0.02 mL/min. At the first fractional flow point ($f_w$=0), only oil was injected at 0.02 mL/min. Then, the water fractional flow was increased to 0.15 with water rates of 0.003 mL/min and oil rate of 0.017 mL/min. The water fractional flow was increased in steps to 100%. At $f_w$=1, the water flow rate was increased (from 0.02 mL/min to 2 mL/min) to reach residual oil saturation, which was then decreased back to 0.02 mL/min at which the pressure drop was measured.

The co-injection of crude oil and formation brine at each water fractional flow continued for at least 20 hr. Two overlapping scans (one hour each) were taken at a stabilized pressure drop at the end of the flow period.
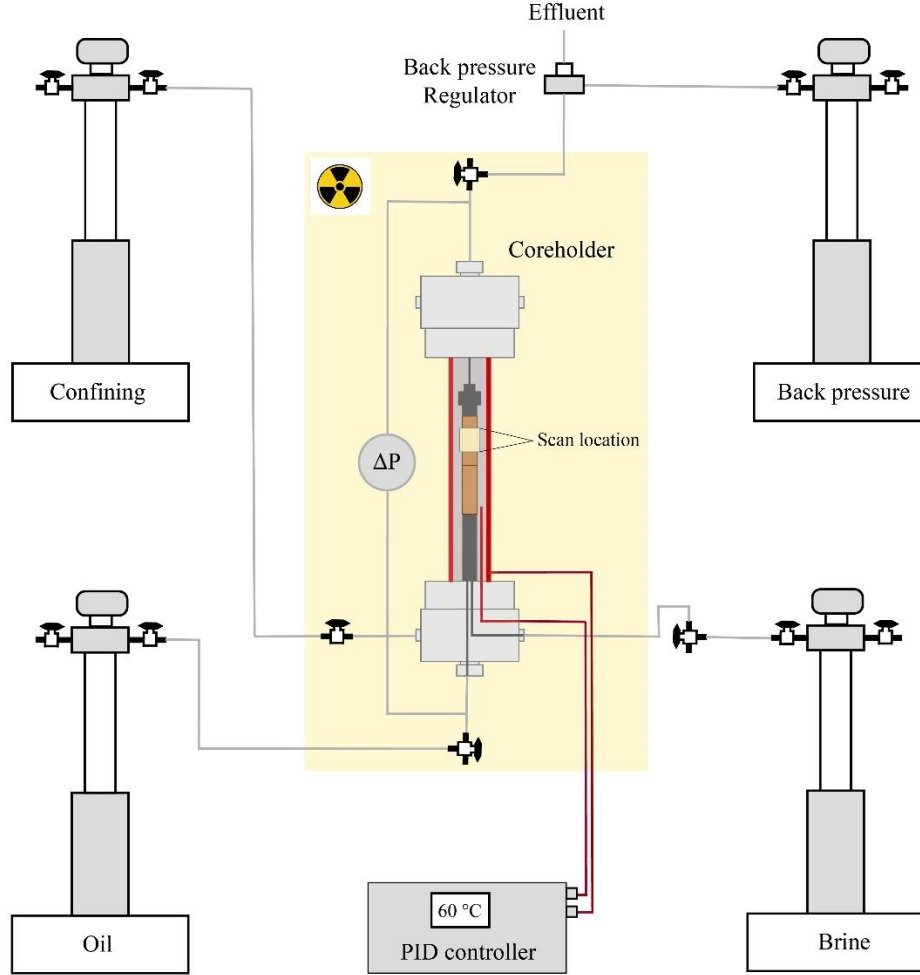
**Fig. 2 :** The high-pressure high-temperature flow apparatus consists of five main components. 1. Core holder assembly. 2. High pressure syringe pumps to control the flow rates, confining pressure and back pressure. 3. Back pressure regulator. 4. PID controller to control the applied temperature. 5. Pressure transducer recording the pressure differential across the sample.

### 2.2.2 Three-dimensional X-ray imaging and image processing.

We used a Zeiss Xradia 510 Versa X-ray micro-tomography scanner to take the high resolution three-dimensional X-ray images. All scans were acquired at an energy and power of 75 keV and 6.5 W, respectively. A flat panel detector was used to obtain a large field of view with a voxel size of 3.567 μm with a total number of projections of at least 3,200 to acquire good quality images. All tomograms were reconstructed using the Zeiss Reconstructor Software and the most appropriate centre shift correction value was applied.

The two overlapping images were all normalized to the brine reference scan and stitched together to form a larger image with a total size of $6 \times 6 \times 9$ mm$^3$, with 7.1 billion voxels. The stitched images were then registered to the stitched dry reference image to have the same spatial orientation that facilitates an accurate fluid quantification at the same location by differential imaging. The grey-scale images were filtered using the non-local means filter [43, 44]. To quantify oil and brine saturation accurately, the differential imaging technique was used [24, 37, 39] to segment the $6 \times 6 \times 9$ mm$^3$ images. This method allows us to quantify oil and brine volumes in small pores that cannot be explicitly resolved in the image. The pore space and rock phases were segmented at the beginning from the difference between the two reference scans (dry and high contrast brine scans). The 30 weight % KI added to brine had an even higher grey-scale value than the solid grains. The difference images were able to identify low density minerals or isolated micro-pores. Then, a two-step watershed segmentation [45] was used to segment solid, micro-porous grains and macro-pores. The next step was to segment the oil phase in macro-pores (pores that could be resolved in the image) and micro-pores (pore space below the image resolution) by applying the image difference between the multiphase scans and the high contrast brine scan. The oil and brine phase were segmented using grey-scale interactive thresholding for all water fractional flows.
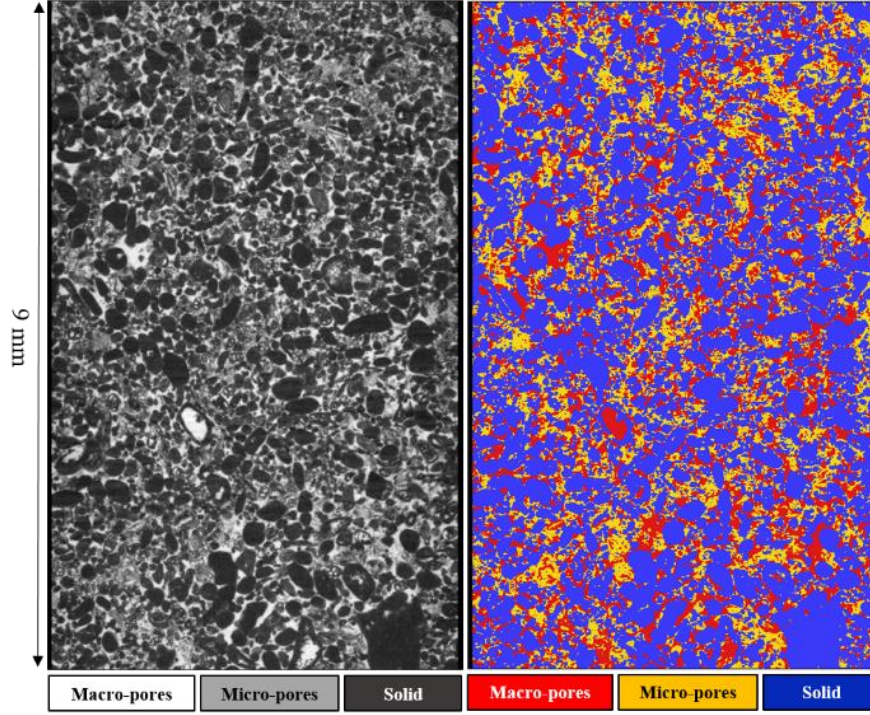
**Fig. 3:** Three-phase segmentation of the rock and pore space. On the left, the difference image between high contrast brine reference scan and the dry scan is presented. On the right, the segmented solid, micro-porous grains and macro-pores are shown.

A smaller sub-volume was extracted with an image size of $2 \times 2 \times 2$ mm$^3$ to measure the oil-brine interfacial curvature from which capillary pressure was calculated. The smaller sub-volume image was segmented using the same method described above, but the image difference was applied between the multiphase scans and the dry reference scan to generate very sharp brine-oil interfaces that could capture the shape of the fluids and interfaces in the pore space.

### 2.2.3 Pore-space characterization

The reservoir rock is made up of a complex and heterogeneous pore space with a wide range of pore sizes from sub-microns to millimetres. To accurately characterize such heterogeneous porous media in 3D, we use differential imaging between the high contrast brine reference scan and the dry reference scan which provides an accurate segmentation of solid, micro-porous grains and macro-pores, Figure 3. The total pore volume was quantified by

$$PV = 1 \times V_{macro} + \phi_{sub} \times V_{micro} \qquad (1)$$

$$\phi_{sub} = \frac{CT_{sub} - CT_{grain}}{CT_{macro} - CT_{grain}} \qquad (2)$$

which is simply the summation of the macro-pore and micro-pore volumes.

The contribution to porosity of the micro-porous space was determined by plotting the histograms for the grey-scale voxels in the brine reference image to find the peak (CT) in each phase and calculating the sub-resolution porosity fraction ($\phi_{sub}$), Figure 4. The total of macro- and micro-porosity measured from X-ray differential imaging was 27.4 % (where the macro-pores contributed 65.8% to the total porosity with 34.2% from the micro-pores) compared to a helium porosity of 27.8 % measured on the 1.5 inch (38 mm) core plug from which the rock sample was drilled. The MICP porosity was 27.0 % measured on a trim of the larger plug. The consistency of these values indicates that we have imaged a representative elementary volume of this rock.
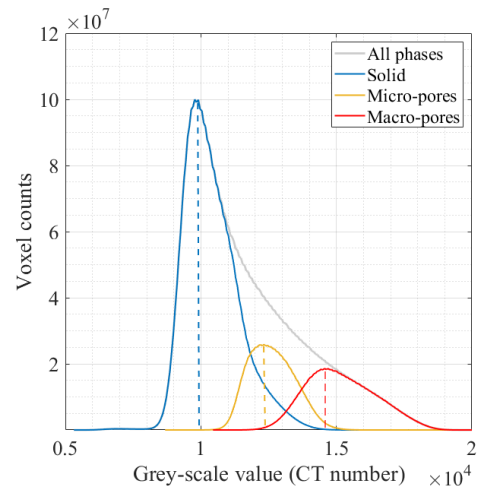


**Fig. 4:** The histograms of the grey-scale voxels in the brine reference image used to calculate the sub-resolution fraction in the micro-porous matrix.
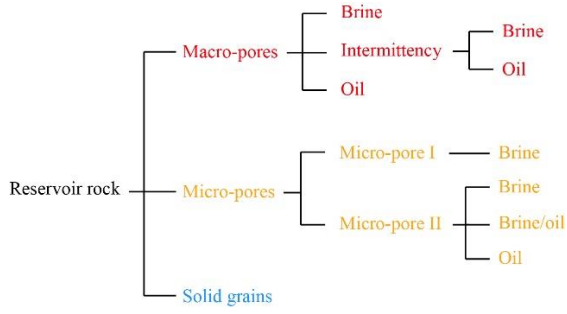
**Fig. 5:** A schematic diagram shows the brine quantification diagram in all phases of the reservoir rock.

### 2.2.4 Water saturation quantification

The water saturation was quantified in both macro-pores (pores that can be resolved by the image resolution) and micro-pores (pores that have sizes smaller than the image resolution). The difference image between the multiphase scans at different fractional flows and the high contrast brine reference image accurately distinguished between the oil and brine phases in micro-and macro pore space. Figure 5 shows a schematic diagram of how the brine and oil were quantified.

Firstly, by differential imaging we were able to distinguish the intermittent phase in macro pores in which both oil and brine periodically existed as a single phase during the one-hour scan. The brine saturation in the intermittent phase that existed in the first two fractional flows was quantified by

$$S_{w\_inter\_macro} = \phi_{inter} \frac{CT_{inter} - CT_{oil}}{CT_{brine} - CT_{oil}} \quad (3)$$

where $\phi_{inter}$ is the fraction of the intermittent phase in the total pore volume. CT refers to the peak grey-scale value found for each phase in the histogram of the raw multiphase image.

Similar to the recent study by Gao et al. [40] on Estaillades limestone we observed that with increased fractional flow some voxels in micro-porosity did not change their grey scale value (their difference image value was zero), while the grey-scale value of other voxels decreased since some of the initially residing oil was displaced. We therefore infer that the former were always occupied by brine as micro-pore phase I, while the latter was micro-porous phase II consisting of both brine and oil. This is illustrated for $f_w$=0.5 in Figure 6.

The brine saturation in micro-pore phase I is equal to the pore space fraction in micro-pore phase I ($\phi_I$) that is fully saturated with brine. Whereas, the brine saturation in micro-pores II is quantified by

$$S_{w\_PF\_micropore II} = \phi_{PFM} \frac{CT_{PFmicropores} - CT_{oil}}{CT_{brine} - CT_{oil}} \quad (4)$$

where $\phi_{PFM}$ represents the fraction of the partially filled micro-pore space. CT refers to the peak grey-scale value found for each phase in the histogram of the raw multiphase image. The quantified brine saturation in macro and micro pore space at fractional flow 0.5 is shown over the length of the sample in Figure 7.
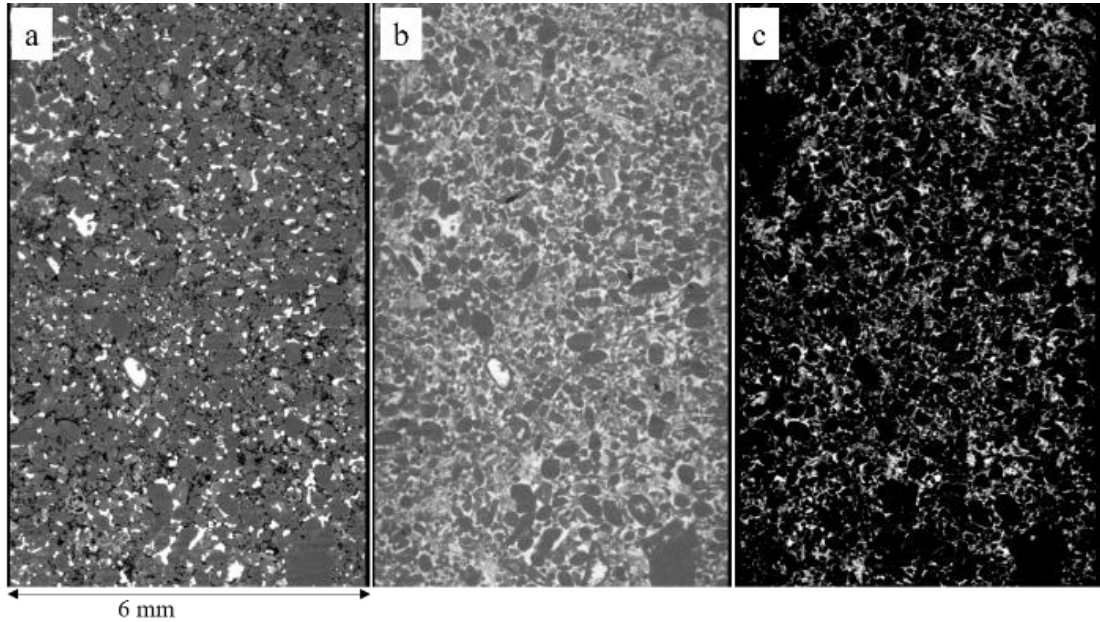


**Fig. 6:** a. Multiphase scan at $f_w$=0.5 where oil, rock and brine are shown in black, grey and white respectively. b. High contrast brine reference scan. c. Difference image between multiphase scan and the high contrast scan, where oil is shown in white and, rock and brine are shown in black.

# 3 Results and Discussion

We focus attention on the measured relative permeability and capillary pressure in the mixed-wet carbonate sample and interpret the behaviour based on the pore occupancy obtained from micro-CT images.
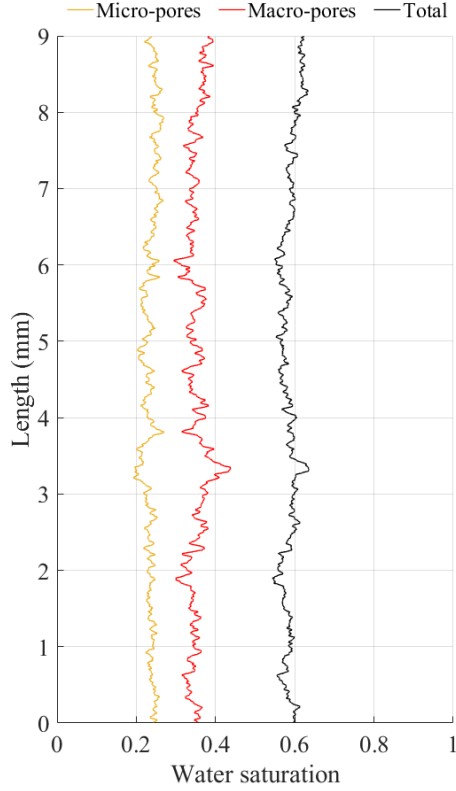


**Fig. 7:** Brine saturation profile of $f_w$=0.5 in macro-pores (red), micro-pores (orange) and total (black).

## 3.1 Relative permeability

The relative permeability of brine and oil were calculated using Darcy's law. The brine saturation at each fractional flow was measured on the segmented X-ray images while the pressure differential across the sample was measured using the pressure transducer. The *in situ* wettability was measured at $f_w$=0.5 on the segmented image showing a mixed-wet system with predominantly oil-wet surfaces with a mean contact angle of 113° ± 20°, [29, 46, 47]. As observed from Figure 8, the brine relative permeability is low and approximately constant until the cross-over point which occurs at $S_w$=63%. This means that, despite increasing fractional flow and saturation of water, there is no increase in water connectivity in the pore space. Approximately just before the cross-over point, water permeability starts to increase and above $f_w$=0.7 rises more steeply to high values, which is an indication of the enhanced connectivity in both macro- and micro-pore space.

The oil relative permeability remains finite after the cross-over point until the residual oil saturation, $S_{or}$ is attained. This is an indicator of oil connectivity at low oil saturations that is achieved through layer flow and has very important implications for favorable oil recovery. This finding is also supported in Figure 9 showing one-dimensional water saturation profiles along the core. We observe a significant additional oil recovery when $f_w$ is increased from 0.95 and 1 to reach residual oil saturation. In addition, significantly higher oil recovery is observed for fractional flow changes between 0 and 0.5, which is consistent with the previously explained observation of approximately constant water relative permeability. More detailed pore-scale observations associated with favorable oil recovery in the mixed-wet carbonate reservoir rock are presented elsewhere [48].
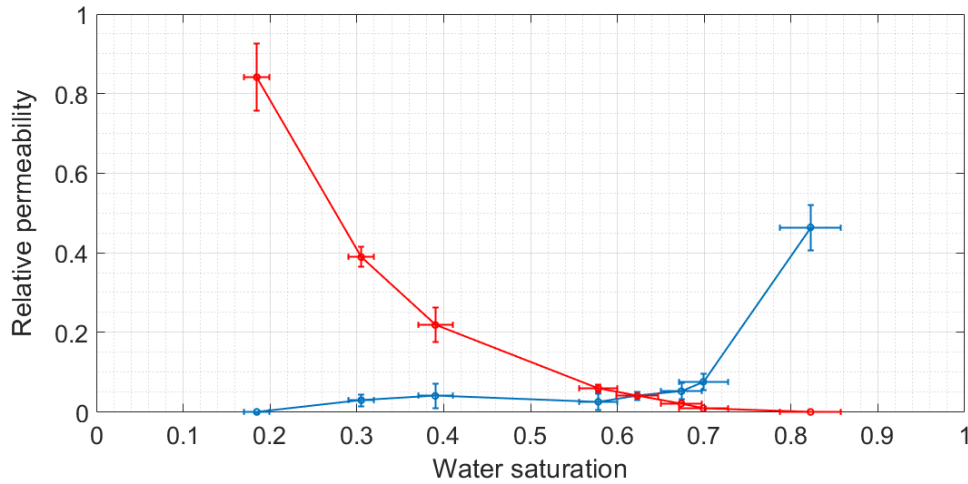


**Fig. 8:** Relative permeability measured for a steady state oil-brine waterflood in the mixed-wet reservoir carbonate sample. The error bars account for pump accuracy that controls flow rates and pressure measurement across the sample, and the uncertainty in the measurement of saturation from the images.
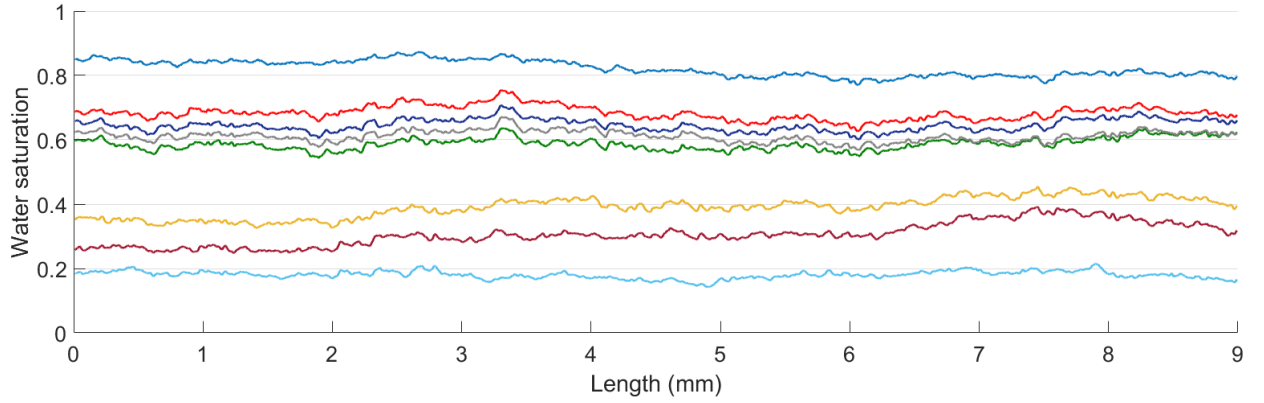
**Fig. 9:** Total brine (water) saturation profiles averaged in slices perpendicular to the flow direction for all of the eight water fractional flows over the length of the analyzed image. The lowest profile is for $f_w$=0 and the top is $f_w$=1.

The pressure differentials across the sample at the eight fractional flows are shown in Table 1. The sample pressure drop gradually increases with fractional flow increase until around the cross-over point. Here the pressure differential is highest as oil and brine have similar saturations and compete to flow through the same pores.

**Table 1.** Pressure differential across the sample at the eight fractional flows. SD indicates standard deviation and represents the fluctuations observed in the pressure recordings.

| $f_w$ | 0 | 0.15 | 0.3 | 0.5 | 0.7 | 0.85 | 0.95 | 1 |
|---|---|---|---|---|---|---|---|---|
| Total pressure drop (kPa) | 6.61 | 10.30 | 18.04 | 42.61 | 40.88 | 36.04 | 25.74 | 5.81 |
| Line pressure drop (kPa) | 2.18 | 2.16 | 6.11 | 10.28 | 13.11 | 9.91 | 5.68 | 2.36 |
| Sample pressure drop (kPa) | 4.43 | 8.14 | 11.93 | 31.33 | 27.77 | 26.13 | 20.06 | 3.45 |
| Sample pressure drop SD (kPa) | 0.13 | 0.22 | 1.89 | 0.36 | 0.32 | 0.29 | 0.25 | 0.13 |

### 3.2 Capillary pressure

Understanding capillary pressure, which controls fluid configurations at the pore-scale is essential to quantify the performance of hydrocarbon reservoirs at the macro-scale. The local capillary pressure was calculated from the measured mean interfacial curvature using the Young-Laplace law

$$P_c = 2\sigma\kappa \qquad (5)$$

The interfacial tension, $\sigma$, was measured to be $27.9 \pm 0.64$ mN/m at 60 °C. The curvature was determined on the smoothed oil/brine interfaces by the average of the two principal curvatures: $\kappa = (\kappa_1 + \kappa_2)/2$, [20, 21, 25, 26]. The brine/oil interfacial curvature at $f_w$=0.5 measured on the sample volume of $2 \times 2 \times 2$ mm$^3$ is shown in Figure 10. We observe both positive and negative values. The curvature histogram of 4.5 million measured values at $f_w$=0.5 is shown in Figure 11, with a negative average value ($-0.011 \pm 0.042$ μm$^{-1}$) which results in the negative capillary pressure of -590 Pa.
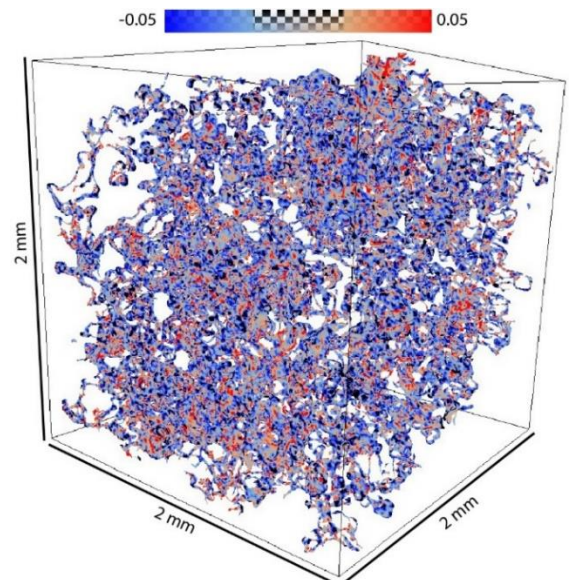


**Fig. 10:** Interfacial curvature (μm$^{-1}$) at $f_w$=0.5 where blue shows negative values and red shows positive values.
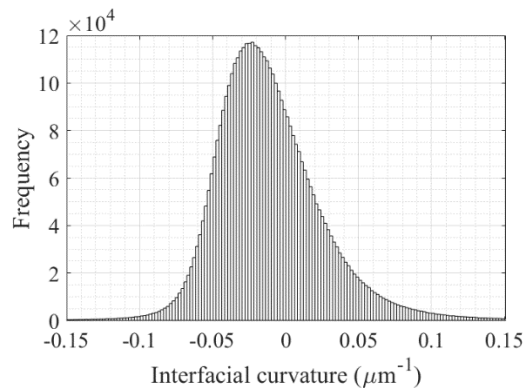
**Fig. 11:** Interfacial curvature distribution of 4.5 million measured values at $f_w$=0.5.

Capillary pressures calculated from the brine/oil interfacial curvature measurements for $f_w$ ranging from 0 to 0.95 are presented in Figure 12. They all have negative values ranging from -150 Pa to -630 Pa. This confirms that the fluid pressures are higher in brine than in oil, which is a characteristic of predominantly oil-wet media. Moreover, capillary pressure decreases with increasing water fractional flow.
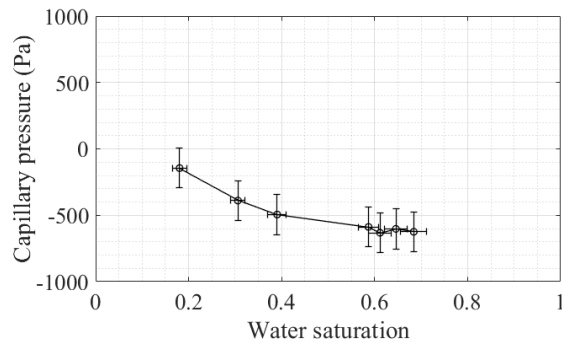


**Fig. 12:** The capillary pressure estimated from the average curvature of the oil-water interfaces plotted as a function of water saturation.

## 4 Conclusions and implications

Relative permeability and capillary pressure were measured simultaneously on a mixed-wet carbonate reservoir rock by conducting a steady-state experiment using crude oil and prepared doped formation brine from the same reservoir at subsurface conditions. Our main conclusions and implications from this work are:

• The relative permeability was measured by using water saturation quantified on X-ray segmented images and by measuring the pressure differential measured across the sample by a pressure transducer. The cross-over of the relative permeability was above 60% indicating favourable oil recovery.

• The capillary pressure was determined from the average of the local interfacial curvature. As expected for a predominantly oil-wet system, the capillary pressure was negative and decreased with increasing water fractional flow.

• Differential imaging was used to quantify fluid saturation in both macro-porosity and micro-porosity (sub-resolution). Hence, this work presents a procedure to perform oil and brine saturation quantification in micro-porous carbonate reservoir rocks, facilitating further studies to quantify oil recovery from macro- and micro-porosity for different reservoir systems.

• The results from this work could be used in future to benchmark pore-scale modelling to enhance the prediction of the multiphase flow in complex carbonate reservoirs

## Acknowledgement

## References

1. M. J. Blunt, "Multiphase flow in permeable media: A pore-scale perspective", *Cambridge University Press* (2017).

2. P. P. Jadhunandan, N. R. Morrow, "Effect of wettability on waterflooding recovery for crude oil/brine/rock systems". *SPE Reservoir Engineering.* **10** (1), 40-46 (1995).

3. S. Bachu, "$CO_2$ storage in geological media: Role, means, status and barriers to deployment". *Progress in Energy and Combustion Science*, **34** (2), 254-273 (2008).

4. M. R. Dernaika, M. A. Basioni, A. M. Dawoud, M. Z. Kalam, S. M. Skjaeveland, "Variations in Bounding and Scanning Relative Permeability Curves With Different Carbonate Rock Type". *SPE Reservoir Evaluation & Engineering*, **16** (3), 265-280 (2013).

5. S. K., Masalmeh, X. D. Jing, W. van Vark, S. Christiansen, H. Van der Weerd, J. Van Dorp, "Impact of SCAL (special core analysis) on carbonate reservoirs: How capillary forces can affect field performance predictions". *Petrophysics,* **45**, 403–413. (2004).

6. J. C. Parker, "Multiphase flow and transport in porous media". *Reviews of Geophysics*, **27**(3), 311 (1989).

7. G. L. Hassler, E. Brunner, "Measurement of capillary pressures in small core samples". *Transactions of AIME*, **160**(01), 114–123 (1945).

8. M. Z. Kalam, K. Al Hammadi, O. B. Wilson, M. Dernaika, H. Samosir, "Importance of porous plate measurements on carbonates at pseudo reservoir conditions", *SCA2006-28, Proceedings of the 2006 SCA International Symposium, Trondheim, Norway.* (2006).

9. S. K. Masalmeh, X. D. Jing, "The importance of special core analysis in modelling remaining oil saturation in carbonate fields". *SCA2008-03. In*

*Proceedings of the International Symposium of the Society of Core Analysis.* (2008).

10. M. R. Dernaika, M. S. Efnik, S. Koronfol, S. M. Skjaeveland, M. M. Al Mansoori, H. Hafez, M. Z. Kalam, "Capillary Pressure and Resistivity Index Measurements in a Mixed-Wet Carbonate Reservoir". *Petrophysics*, **55**(01), 24-30 (2014).

11. M Kennedy, "Practical petrophysics". *Netherlands: Elsevier* (2015).

12. C. McPhee, J. Reed, I. Zubizarreta, "Best practice in coring and core analysis". *In Developments in Petroleum Science,* 1–15 (2015).

13. D. Wildenschild, A. P. Sheppard, "X-ray imaging and analysis techniques for quantifying pore-scale structure and processes in subsurface porous medium systems". *Advances in Water Resources*. **51**, 217-246. (2013).

14. M. Andrew, B. Bijeljic, M. J. Blunt, "Pore-scale imaging of geological carbon dioxide storage at in situ conditions". *Geophysical Research Letters*. **40**, (15), 3915-3918 (2013).

15. M. J. Blunt, B. Bijeljic, H. Dong, O. Gharbi, S. Iglauer, P. Mostaghimi, A. Paluszny, C. Pentland, "Pore-scale imaging and modelling". *Advances in Water Resources*, **51**, 197–216 (2013).

16. S. Berg, H. Ott, S. Klapp, A. Schwing, R. Neiteler, N. Brussee, A. Makurat, L. Leu, F. Enzmann, j. Schwarz, M. Kersten, S. Irvine, M. Stampanoni, "Real-time 3D imaging of Haines jumps in porous media flow". *Proceedings of the National Academy of Sciences*. **110**, (10), 3755-3759 (2013).

17. S. Schlüter, A. Sheppard, K. Brown, D. Wildenschild, "Image processing of multiphase images obtained via X-ray microtomography: a review". *Water Resources Research*. **50**, (4), 3615-3639 (2014).

18. C. A. Reynolds, H. Menke, M. Andrew, M. J. Blunt, S. Krevor, "Dynamic fluid connectivity during steady-state multiphase flow in a sandstone". *Proceedings of the National Academy of Sciences*. **114**, (31), 8187-8192 (2017).

19. A. M. Alhammadi, A. AlRatrout, B. Bijeljic, M. J. Blunt, "Pore-scale Imaging and Characterization of Hydrocarbon Reservoir Rock Wettability at Subsurface Conditions Using X-ray Microtomography". *Journal of Visualized Experiments*, (140), e57915 (2018).

20. R. T. Armstrong, M. L. Porter, D. Wildenschild, "Linking pore-scale interfacial curvature to column-scale capillary pressure". *Advances in Water Resources*, **46**, 55–62 (2012).

21. K. Singh, H. Menke, M. Andrew, Q. Lin, C. Rau, M.J. Blunt, B., Bijeljic, "Dynamics of snap-off and pore-filling events during two-phase fluid flow in permeable media". *Scientific Reports*. **7**, (1), 5192 (2017).

22. A. L. Herring, L. Andersson, D. Wildenschild, "Enhancing residual trapping of supercritical $CO_2$ via cyclic injections". *Geophysical Research Letters*. **43**, (18), 9677-9685 (2016).

23. A. L. Herring, J. Middleton, R. Walsh, A. Kingston, A. Sheppard, "Flow rate impacts on capillary pressure and interface curvature of connected and disconnected fluid phases during multiphase flow in sandstone". *Advances in Water Resources*, **107**, 460–469 (2017).

24. Y. Gao, Q. Lin, B. Bijeljic, M. J. Blunt, "X-ray Microtomography of Intermittency in Multiphase Flow at Steady State Using a Differential Imaging Method". *Water Resources Research* **53**, 10274–10292 (2017).

25. M. Andrew, B. Bijeljic, M. J. Blunt, "Pore-by-pore capillary pressure measurements using X-ray microtomography at reservoir conditions: Curvature, snap-off, and remobilization of residual $CO_2$". *Water Resources Research*, **50**, 8760–8774. (2014a).

26. Q. Lin, B. Bijeljic, R. Pini, M. J. Blunt, S. Krevor, "Imaging and measurement of pore-scale interfacial curvature to determine capillary pressure simultaneously with relative permeability". *Water Resources Research*, **54**(9), 7046-7060 (2018).

27. R. A. Salathiel, "Oil recovery by surface film drainage in mixed-wettability rocks". *Journal of Petroleum Technology*. **25**, 1216–1224 (1973).

28. A. R. Kovscek, H. Wong, C. J. Radke, "A pore-level scenario for the development of mixed wettability in oil reservoirs". *AIChE J.* **39**, 1072–1085 (1993).

29. A. M. Alhammadi, A. AlRatrout, K. Singh, B. Bijeljic, M. J. Blunt, "In situ characterization of mixed-wettability in a reservoir rock at subsurface conditions". *Scientific Reports*, **7**(1), 10753 (2017).

30. J. S. Buckley, Y. Liu, S. Monsterleet, "Mechanisms of wetting alteration by crude oils". *SPE Journal*. **3**, 54–61 (1998).

31. W. G. Anderson, "Wettability literature survey-part 2: Wettability measurement". *Journal of Petroleum Technology*. **38**, (11), 1246-1262 (1986).

32. Anderson, W. G. "Wettability literature survey - part 5: The effects of wettability on relative permeability". *Journal of Petroleum Technology*. **39**, (11), 1453-1468 (1987a).

33. W. G. Anderson, "Wettability literature survey - part 6: The effects of wettability on waterflooding". *Journal of Petroleum Technology*. **39**, (12), 1605-1622 (1987b).

34. L. E. Cuiec, "Evaluation of reservoir wettability and its effect on oil recovery". *Interfacial Phenomena in Petroleum Recovery*. 319-375 (1990).

35. Morrow, N. R. "Wettability and its effect on oil recovery". *Journal of Petroleum Technology*. **42**, (12), 1476-1484 (1990).

36. S. Zou, R. T. Armstrong, J. Y. Arns, C. H. Arns, F. Hussain, "Experimental and Theoretical Evidence for Increased Ganglion Dynamics During Fractional Flow in Mixed-Wet Porous Media". *Water Resources Research*. **54** (5), 3277-3289 (2018).

37. Q. Lin, Y. Al-Khulaifi, M.J. Blunt, B. Bijeljic, "Quantification of sub-resolution porosity in carbonate rocks by applying high-salinity contrast brine using X-ray microtomography differential imaging". *Advances in Water Resources*, **96**, 306–322 (2016).

38. B. Bijeljic, A. Q. Raeini, Q. Lin, M. J. Blunt, "Multimodal Functions as Flow Signatures in Complex Porous Media" (2018). arXiv Prepr. arXiv1807.07611.

39. Q. Lin, B. Bijeljic, H. Rieke, M. J. Blunt, "Visualization and quantification of capillary drainage in the pore space of laminated sandstone by a porous plate method using differential imaging X-ray microtomography". *Water Resources Research* **53**, 7457–7468 (2017).

40. Y. Gao, A. Q. Raeini, M. J. Blunt, B. Bijeljic, "Pore Occupancy, Relative Permeability and Flow Intermittency Measurements Using X-Ray Micro-tomography in a Complex Carbonate", *Advances in Water Resources*, **129**, 56-69 (2019).

41. P. L. Gant, W. G. Anderson, "Core cleaning for restoration of native wettability", *SPE Formation Evaluation*, **3**(1), 131–138 (1988).

42. M. Andrew, B. Bijeljic, M. J. Blunt, "Pore-scale imaging of trapped supercritical carbon dioxide in sandstones and carbonates". *International Journal of Greenhouse Gas Control*. **22**, 1-14 (2014b).

43. A. Buades, B. Coll, J. M. Morel, "A non-local algorithm for image denoising". *Proceedings / CVPR, IEEE Computer Society Conference on Computer Vision and Pattern Recognition*. **2** (7), 60-65 (2005).

44. A. Buades, B. Coll, J. M. Morel, "Nonlocal image and movie denoising". *International Journal of Computer Vision*. **76** (2), 123-139 (2008).

45. A.C. Jones, C.H. Arns, A.P. Sheppard, D.W. Hutmacher, B.K. Milthorpe, M.A. Knackstedt, "Assessment of bone ingrowth into porous biomaterials using micro-CT". *Biomater*. **28**, 2491–2504 (2007).

46. A. AlRatrout, M. J. Blunt, B. Bijeljic, "Wettability in complex porous materials, the mixed-wet state, and its relationship to surface roughness". *Proceedings of the National Academy of Sciences*, **115** (36), 8901-8906 (2018).

47. A. AlRatrout, A. Q. Raeini, B. Bijeljic, M. J. Blunt, "Automatic measurement of contact angle in pore-space images". *Advances in Water Resources*. **109**, 158-169 (2017).

48. A. M. Alhammadi, Y. Gao, T. Akai, M. J. Blunt, B. Bijeljic, "Pore-scale X-ray imaging with measurement of relative permeability, capillary pressure and oil recovery in a mixed-wet micro-porous carbonate reservoir rock". *Fuel* (Under Review) (2019).